Carbon Nanotube Membranes: From flow enhancement to permeability

Davide Mattia,* Hannah Leese, and Kah Peng Lee

Department of Chemical Engineering, University of Bath, BA27AY, UK

*corresponding author: d.mattia@bath.ac.uk
phone: +44-(0)1225-383961

Abstract:

Since their discovery, carbon nanotubes have been considered as a potential material for filtration applications due to low tortuosity, smooth structure and the possibility of fine tuning their diameter. Measurements of fluid flow in nanotubes, with diameters ranging from 0.6 to 100 nm dramatically raised interest in them, with very high water flow rates promising to deliver orders-of-magnitude higher performance compared to other membranes. This promise was based on reports of flow enhancement, defined as a ratio of the measured flow compared to a no-slip Poiseuille flow, ranging from 10 to 100,000 with the underlying assumption that commercial membranes would exhibit the no-slip behavior. The concept of flow enhancement, though, is of little help for actual filtration applications where one is interested in a membrane's performance in terms of selectivity and permeability. In this work, the flow enhancement and permeability of UF carbon nanotube – anodic alumina membranes (CNT-AAM) with a large range of diameters is reported. Using a recently developed model, it is shown that the permeability is directly related to the solid-liquid molecular interactions between the liquid and the nanotubes. Finally, the performance of these CNT membranes and others in the literature has been analyzed in terms of permeability, comparing them to commercial membranes in the RO, NF and UF ranges. Results show that in fact, carbon nanotube membranes have a higher pure water permeability than commercial polymer membranes.

keywords: carbon nanotube membrane; flow enhancement; permeability; anodic alumina membrane; ultrafiltration;

1. Introduction

Since their discovery in 1991, carbon nanotubes have been considered as a potential material for filtration applications due to low tortuosity, smooth structure and the possibility of fine tuning their diameter [1]. In the early 2000s measurements of fluid flow in nanotubes, with diameters ranging from 0.6 to 100 nm dramatically raised interest in them, with very high flow values reported for both liquids and gases [2]. High water flow rates, in particular, promised to deliver orders-of-magnitude higher performance compared to commercial membranes. This promise was based on reports of flow enhancement, defined as the ratio of the measured flow compared to a no-slip Poiseuille flow, ranging from 10 to 100,000 [2] and the underlying assumption that commercial membranes would exhibit no-slip behavior. A vast literature now exists on flow enhancement in nanotubes either as individual or in membrane configuration, with both experimental and modeling studies. Furthermore, numerous theoretical models have been developed to try to explain this apparent unusual behavior.

The concept of flow enhancement, though, is of little help for actual filtration applications where one is interested in a membrane's performance in terms of selectivity and permeability. Numerous studies on flow enhancement in carbon nanotubes, particularly modeling, do not report the necessary information to calculate permeability and very few have looked at selectivity.

Additionally, there are still significant problems with the manufacturing methods for carbon nanotube membranes, all concerning alignment of the nanotubes. Methods based on aligned forests of nanotubes produced via chemical vapor deposition can produce high quality small membranes (~1 cm^2) with a polymer [3-6] or ceramic [7] matrix embedding the tubes to prevent leaks or as a dense membrane [8]. Unfortunately these technologies are not scalable as they require expensive substrates (ex. silicon wafers) and vacuum-based processes [9]. In these membranes, often referred to as VA-CNT membranes, the tubes are directly exposed to the liquid to filter and filtration occurs mainly via steric hindrance and follows the pore flow model. Numerous attempts at incorporating nanotubes in the active layer of thin film composite membranes have yielded mixed results, mainly due to the challenge of uniformly aligning the tubes perpendicularly to the membrane surface. Nonetheless, single-digit improvements in permeability, compared to virgin membranes without tubes, have been obtained for membranes containing randomly aligned tubes, where it can be assumed a certain fraction of tubes will be oriented in a direction favorable to enhance flow [10-13]. In all these membranes, identified as (CNT-TFC), selectivity is still determined by the polymer active layer, whereas the embedded CNTs act as internal 'fast lanes' for water flow once it has entered the membrane.

A recent analysis has put to rest the claim that a high flow enhancement could simply be translated into higher performance membranes. In particular for seawater desalination, where RO plants already perform very close to the thermodynamic limit [14], no significant performance increase, in terms of energy per metre cube of water (kWh m^{-3}) treated can be achieved [15]. This is due to the simple fact that the minimum energy needed to pump water through the membrane is determined by the osmotic pressure and is positively related to the recovery rate. Nonetheless, a reduction in the membrane surface needed to treat the same volume of water could be achieved due to higher permeability, reducing the overall plant footprint and costs associated with membrane cleaning. In addition, in NF and UF, where processes are not necessarily as optimized as in RO, additional performance improvements can still be achieved. Finally, the surface chemistry [16] and structure [17] of nanotubes can be controlled to an extent not easily matched by many polymeric membranes, and there are now numerous reports in the literature showing how they can be modified to exhibit anti-bacterial or anti-fouling behavior [18] or high selectivity to specific ions [19].

In this paper, the flow enhancement of UF carbon nanotube membranes with a large range of diameters is reported. The preparation method for these membranes bypasses all tube alignment issues by using a ceramic template to obtain uniform and high quality CNT membranes with all

tubes aligned perpendicularly to the membrane surface. Furthermore, the results are explained using a model recently introduced by the authors, which predicts the permeability of the nanotube membrane based on solid-liquid molecular interactions between the liquid and nanotubes. Finally, the performance of these CNT membranes and others in the literature has been analyzed in terms of permeability, comparing them to commercial membranes in the RO, NF and UF ranges.

2. Materials and Methods

2.1 Synthesis of CNT-AMM membranes

Anodic alumina membranes (AAM) were used as templates for the production of carbon nanotube membranes by non-catalytic chemical vapor (CVD) deposition. The AAMs were produced according to a known technique, described in detail in [20]. Briefly, a high purity aluminum foil (Alfa Aesar) was pre-conditioned (annealed, degreased and electropolished) to obtain a smooth, uniform surface (Figure 1a). Subsequently, the Al film was used as anode in an electrochemical bath and subject to a so-called two-step anodization process. As a voltage is applied to the electrodes, a complex set of reactions occurs at the anode with the Al metal being converted in a porous alumina structure [21]. Control over the applied voltage, electrolyte type and concentration, bath temperature and process time, yields AAMs of different thickness and pore diameter. Under the appropriate conditions, the resulting AAMs have cylindrical pores with constant circular-cross section along the membrane thickness and narrow pore size distribution (Figure 1b) [20]. AAMs can be produced in flat sheet or tubular geometries, with the latter having good potential for scale-up [22].Removal of the remaining aluminum and pore opening then yields and open-through AAM (Figure 1c). Once formed, the AAMs were slowly (1 °C/min) annealed to 900 °C. This is a critical step as alumina undergoes several phase transitions in this temperature range with significant changes in the thermal expansion coefficient. Absence of annealing will induce warping and eventually disintegration of the AAM during the CVD process to fabricate the CNT membranes [17].

The annealed AAMs were then inserted in a quartz tube reactor using quartz rings to hold them in place and perpendicular to the tube axis. The reactor was then placed in a tubular furnace, sealed and heated up to 670 °C at 10 °C/min under 50 sccm of argon. Once the set temperature was reached, the flow was switched to a mixture of ethylene and argon (30:70 volume ratio) for a total flow ranging from 20 to 120 sccm and kept for 2-10 hours. At the chosen reaction temperature, ethylene decomposes and a conformal coating of solid carbon is deposited on the outer surface and inner pores of the template, resulting in the formation of a carbon nanotube membrane (Figure 1d). The thickness of the carbon coating (which is equal to the CNT wall thickness) is linearly dependent on the length of the CVD process [17]. However, at flow rates below 60 sccm, a dense layer of amorphous carbon was formed, blocking the pores. Flow rates and reaction time were varied to change the thickness of the carbon coating, thereby varying the ultimate diameter of the inner bore of the CNT membrane (details in Table S1). At the end of the reaction period, the CNT membranes were allowed to cool under argon flow until room temperature was reached.

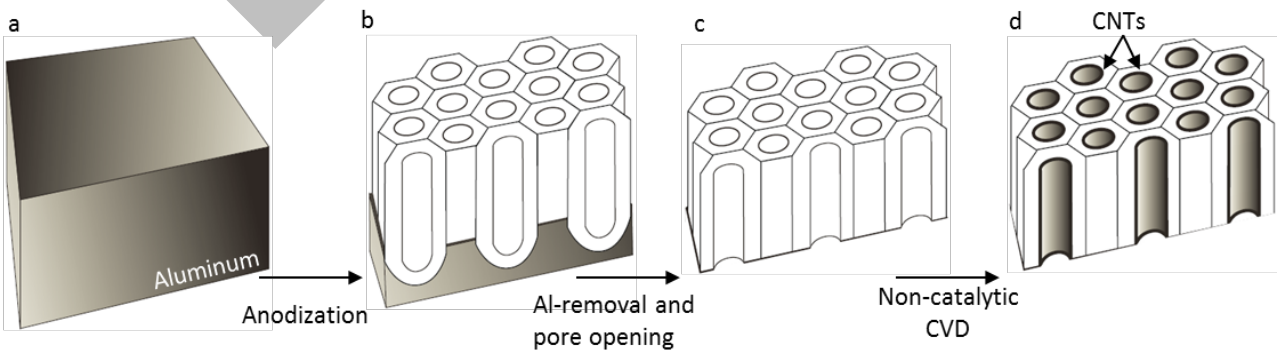

Figure 1. Schematic of the formation of AAM-CNT membranes, starting from metallic Al (a) which is anodized to form a hexagonal pore structure (b); removal of the back laye aluminum and opening of the pores leads to an

open-through AAM (c); non-catalytic CVD deposits a uniform layer of turbostratic graphitic carbons in the AAM pores, forming a nanotube membrane with uniform pore size.

2.2 Characterization of CNT-AMM membranes

The CNT membranes were characterized using a field emission scanning electron microscope (FEI Supra 50 and JEOL FESEM) to evaluate porosity (due to the regular cross-section and absence of internal branching [20], surface porosity is representative of the porosity of the whole membrane), membrane thickness, tortuosity and pore size distribution. All values were evaluated by statistical image analysis of SEM micrographs using ImageJ software. Details of the measurement method are reported elsewhere [20]. Raman measurements were conducted using a Renishaw inVia Raman microscope with green laser (514 nm) at reduced power (10%) so as not to alter the tubes' structure.

The wetting behavior of the nanotube membranes was evaluated using a known methodology [16]: Polished disks (1 cm diameter) of high quality dense α-alumina (Pi-kem Ltd.) were cleaned by sonication in acetone and then gently dried with an argon flow. The disks were then placed in the CVD furnace and subject to the same CVD reaction conditions as the AAM templates. Once cooled, contact angle measurements were performed to evaluate the effect of different synthesis conditions on the work of adhesion, the energy required to separate the solid and liquid surface and generate two new interfaces. The measured contact angles vary from 61±2° to 91±2° (individual values reported in Table S1), with an average of 82°, in very good agreement with literature values [2]. The work of adhesion is a measure of the strength of the interaction between the liquid and solid [23] and will be used later to analyze results [24]. Contact angle and work of adhesion measurements were performed using an OCA 15 goniometer (Dataphysics) and the results reported are the average of three measurements.

Flow enhancement and permeability measurements were performed on a custom-made rig consisting of a pressurized liquid reservoir connected to a membrane holder [25]. Pressure transducers were placed at the feed and permeate sides of the membrane to measure the pressure drop. Permeate flow rate was analyzed using a balance (0.001 g). Temperature was measured to account for changes in viscosity. All data was recorded using a bespoke Labview programme.

3. Results and discussion

3.1 Characteristics of CNT-AMMs

SEM analysis confirmed the regular structure of the AAM templates and the formation of carbon nanotubes within the pores of the membrane (Figure 2). All membranes exhibited a tortuosity ~1 and constant cross-section throughout the entire membrane length [22]. The non-catalytic CVD method employed produces a uniform coating throughout the whole length of the template, therefore the length of the carbon nanotubes equals that of the AAM template [16, 17, 26].

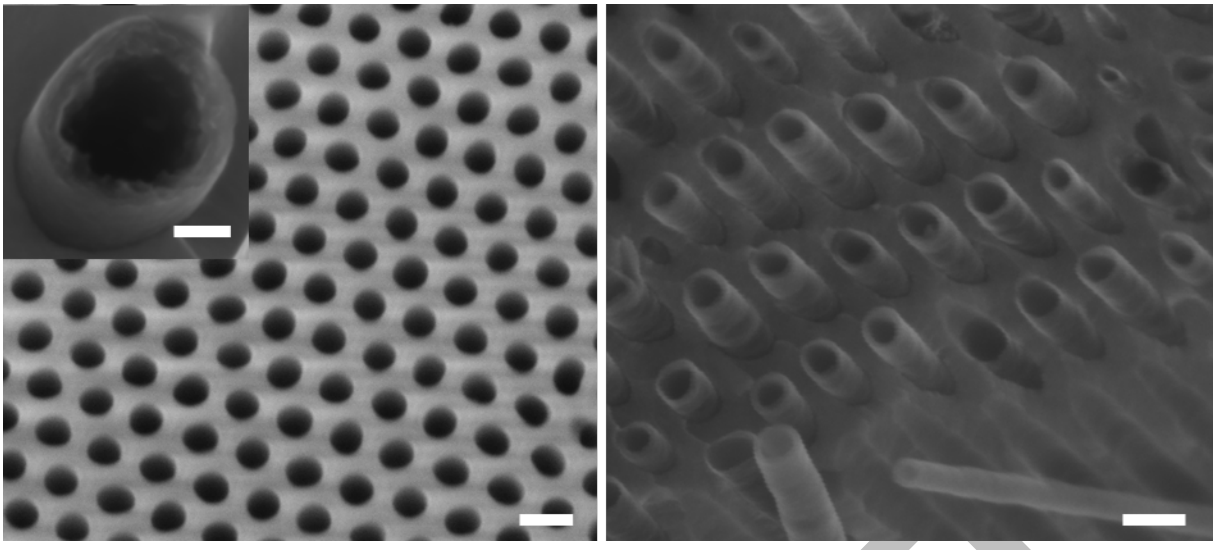

Figure 2. SEM micrographs of the AAM template surface (left) and of CNTs protruding out from a fractured CNT-AMM (right). The inset shows a top view of a CNT with thick wall. Scale bar is 20 nm for all micrographs.

Raman analysis of the nanotubes produced at different conditions showed no structural differences [17], mainly because CVD temperature was not changed. The walls of the CNTs produced using the non-catalytic CVD process described earlier are made of turbostratic graphitic carbon, made up of overlapping small patches of sp^2 carbon [17], which explains the broad D-band in the Raman spectra (Figure 3) [16]. Due to their disordered structures, these CNTs have sometimes been called 'carbon nanopipes' [16, 27] to distinguish them from multi-wall nanotubes, which have an ordered graphitic structure. The formed can be converted into the latter by high temperature annealing in vacuum [17].

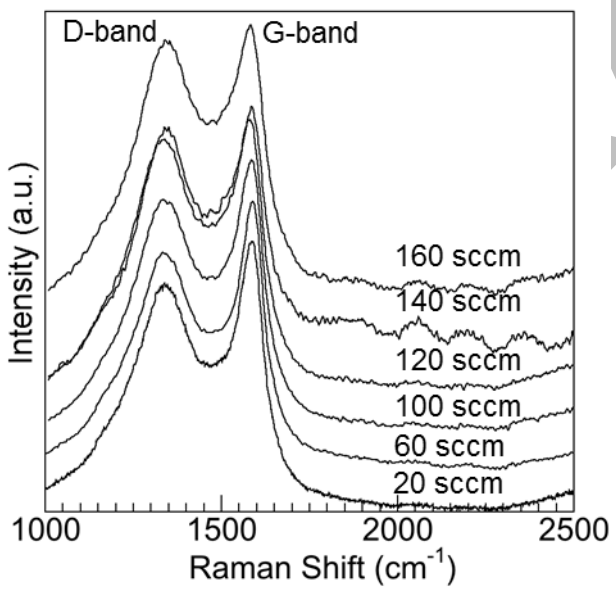

Figure 3. Raman spectra of the CNT-AAMs produced using different CVD precursor gas total flow rates, showing no major structural difference (process details in Table S1).

Work of adhesion (W_A) measurements show relatively small variations, with values ranging from 90 to 110 mJ m^{-2}, compared to a value of 97 for the basal plane of highly ordered graphite. These values are somewhat smaller than the ones (~ 140 mJ m^{-2}) previously calculated for so-called carbon nanopipe membranes synthesized via a similar technique [24]. The difference can be attributed to variation in the surface chemistry and structure of the carbon walls formed during CVD

[24].The measured W_A values have been incorporated in the calculations below and are reported in Table S1 for each nanotube membrane tested.

3.2 Flow Enhancement in CNT-AMMs

The conventional way adopted so far to discuss water flow in CNTs is in terms of flow enhancement, rather than permeability or flux values. The flow enhancement is defined as the positive deviation of the measured flow rate from the no-slip Haagen-Poiseuille case for a steady state flow of an incompressible fluid in a constant cross-section cylindrical channel:

$$\varepsilon = \frac{Q_{\exp}}{Q_{HP}} = 1 + 4\frac{\lambda}{R} \quad (1)$$

where λ is the slip length, arising from the Navier boundary condition, which is used as a measure of the deviation from ideality (Q_{HP}, no-slip Haagen-Poiseuille) of the actual flow ($Q_{\exp}$) [28]. An infinite slip length would correspond to a perfect plug flow in the channel [29].

For the CNT membranes produced in this work, the flow enhancement values are shown in Figure 3 inset (values in Table S1). In Figure 4, these values are compared with selected literature data for both experimental and modeling investigation of pure water flow in individual CNTs and in CNT membranes. The absence of any clear trend in the flow enhancement as a function of tube diameter is notable, although higher enhancements are generally obtained for smaller tube diameters (values used and corresponding literature references are in Table S2).

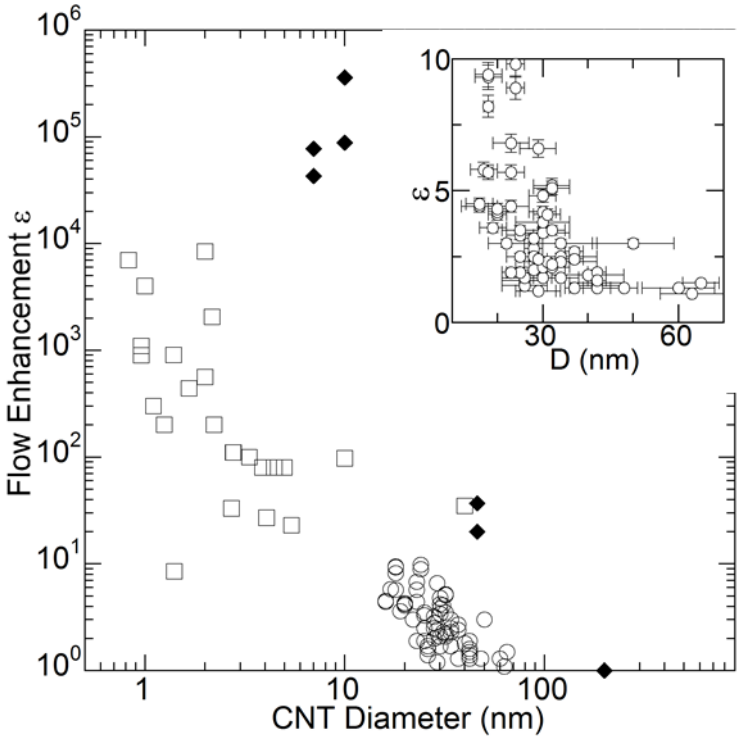

Figure 4. Selected pure water flow enhancement as a function of average CNT diameter for literature data (♦experimental and □ simulations) and for the CNT membranes in the present work (○), log-log plot; references and data for the plot are reported in Table S2. Inset shows the pure water flow enhancement as a function of average CNT diameter produced in this work (compounded error on enhancement 5% of value, arising from measurement accuracy; error on tube diameter reported in Table S1).

The approach discussed above has two main limitations: First, it does not allow comparing results from different publications using nanotubes with different surface chemistry or structure, length and diameter. Second, it does not provide direct information about the membrane's performance to compare with other membranes, polymeric or ceramic.

The first limitation has been addressed by the authors in a previous publication, where a model for the flow enhancement as a function of the tubes' geometric characteristics (radius *R* and length *L*) and solid-liquid molecular interactions has been derived and validated against experimental and modeling results [24, 30, 31]:

$$\varepsilon = \left(\frac{R-\delta}{R}\right)^4 \left(1-\frac{\mu_B}{\mu_W}\right) + \frac{\mu_B}{\mu_W}\left(1+8\mu_W \frac{L}{R^2}\frac{D_s}{W_A}\right) \quad (2)$$

This equation is based on the assumption that there is an annular region near the wall where the liquid exhibits a reduced viscosity due to the concurrent effects of solid-liquid molecular interactions and nanometer scale confinement [32, 33]. This assumption is consistent with results from molecular dynamics (MD) simulations in nanotubes of different size and surface chemistry and structure [34], and has been recently validated for other nanotube materials [31]. δ is the thickness of the low viscosity annular region near the wall and has a fixed value of 0.5 nm, following results from MD simulations [34]; W_A (J m^{-2}) is the work of adhesion [23] and was measured via contact angle experiments for each membrane. D_s (m^2 s^{-1}) is the axial surface diffusion arising from the chemical potential difference due to the applied pressure gradient, and is assumed to be equal to $1 \cdot 10^{-9}$ $m^2 s^{-1}$, following MD results [24, 35]. μ_B is the liquid bulk viscosity and μ_W is the reduced viscosity of the liquid annular region near the wall affected by the nanoscale confinement and interaction with the channel wall, and is assumed here to be equal to 70% of the bulk value, following MD results [24, 33]. As a result, there are no fitting parameters in Eq.(2). A complete derivation of Eq.(2) and discussion about the effect of variations in the values of each term can be found in [24]. The ratio D_s/W_A is a measure of interaction strength between the liquid molecules and tube wall. For a highly hydrophobic material, such as PTFE, D_s is high, W_A low, producing high flow enhancement [24]. Conversely, for a hydrophilic wall, D_s is low [36], W_A high [23, 24] producing a low enhancement, though still nominally higher than 1 [24]. The term W_A is directly related to how the liquid wets the tube walls and incorporates the effects of surface roughness and chemical inhomogeneities [23].

Both can be independently measured. This is a key point as the nanotubes used in many experimental studies on flow in CNT membranes differ dramatically from the ideal, smooth, perfect tubes used in MD studies. For example, low flow enhancements obtained by [37] can be associated with the fact that the tubes used, dubbed nanopipes, have a disordered carbon structure and are rich in functional groups, resulting in a higher W_A value than, for example water in contact with highly graphitized tubes as in [4]. This is further supported by a recent MD study showing that the presence of defects lowers the overall flow enhancement compared to a perfect nanotube [38].

By applying the model in Eq 2 to the membranes in this work and to data in the literature, these become comparable, and the physical dependencies of flow enhancement become apparent (Figure 5). The values of all the quantities used in Eq.(2) to construct the data in Figure 4 are reported in Table S2.

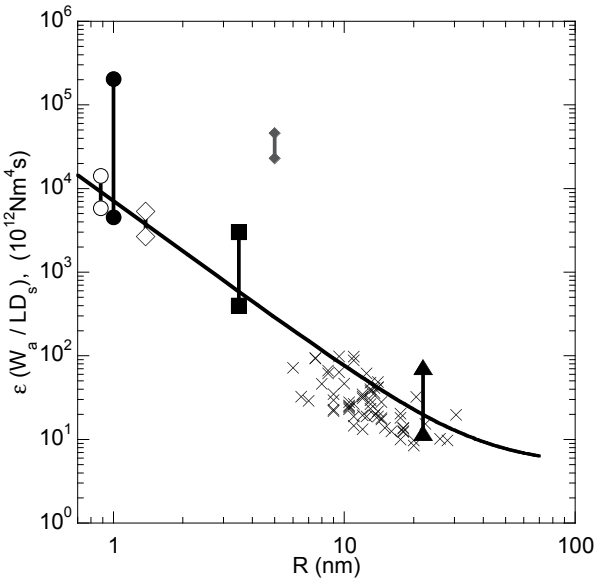

Figure 5. Normalized flow enhancement as a function of nanotube diameter: The solid line is given by Eq. (2) whereas the other symbols are for data published in the literature (♦ [5], • [7], ◊ [32], ○ [33], ■ [4], ▲[37]) and for nanotube membranes produced in this work (x). The normalization allows comparing the flow enhancement for nanotube membranes with different surface chemistry and structure and different length.

3.3 Permeability of CNT-AMMs

Comparison among membranes is generally done in terms of permeability or flux. For the CNT membranes produced in this work, the regular pore structure and narrow pore size distribution of the alumina templates combined with the conformal carbon coating obtained from the CVD process, allows one to define the membranes' porosity as:

$$\phi = \frac{1}{A_{mem}} \sum_{i=1}^{n} \pi R_i^2 \equiv \frac{n\pi R^2}{A_{mem}} \tag{3}$$

where A_{mem} is the membrane area and n the number of pores/CNTs. With this assumption, the total membrane flow rate can be calculated following the model used to derive Eq.(2), and hence, the permeability as:

$$K = \frac{Q}{\Delta P A_{mem}} = \frac{\phi R^2}{8\mu_B L}\left[\left(\frac{R-\delta}{R}\right)^4\left(1-\frac{\mu_B}{\mu_W}\right)+\frac{\mu_B}{\mu_W}\left(1+8\mu_W\frac{L}{R^2}\frac{D_s}{W_A}\right)\right] \tag{4}$$

The first term in the square brackets on the right hand side of the equation is negligible compared to the second one for pore sizes in the ultrafiltration range [24]. In addition $8\mu_W \frac{L}{R^2}\frac{D_s}{W_A} >> 1$ for the same pore size range. Therefore, Eq. (4) can be simplified to:

$$K \approx \phi \frac{D_s}{W_A} \tag{5}$$

There is a good correlation (R^2=0.70) with the experimental permeability for the CNT membranes in this work (Figure 6). Regardless of the membrane pore structure, Eq. (5) relates the permeability of a membrane to the strength of the solid-liquid molecular interactions, via two quantities that, as discussed, can be independently measured using experimental and modeling techniques. In principle, the permeability of any liquid through any membrane could be predicted only knowing the

value of the three terms in Eq. (5). As most membranes have a wider pore size distribution than AAMs as well as tortuosity larger than 1, Equations (3) and (4) would have to be modified accordingly.

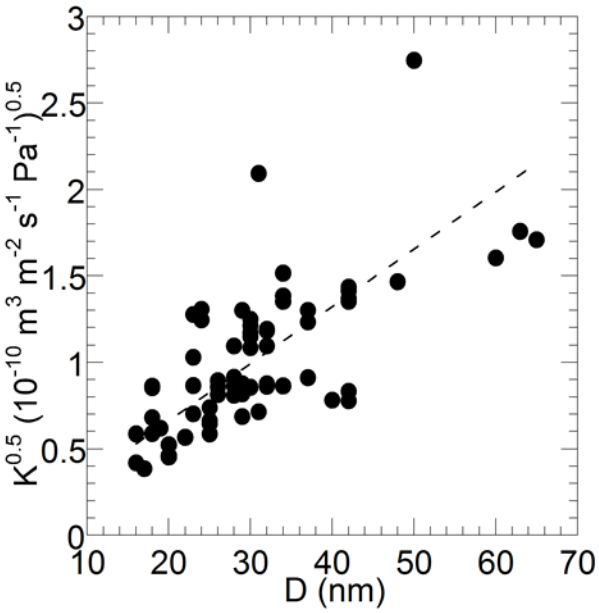

Figure 6. Square root of the permeability for the CVD CNT membranes. The full line is obtained as a fitting of data using Eq.(5), not the experimental permeability data. Values used for specific porosity, work of adhesion and surface diffusion for all CNT membranes tested are in Table S1.

3.4 Comparison with commercial membranes

The permeability for the CNT membranes in this work and selected ones from the literature (the main selection criteria being the availability of all values needed to calculate K) has been plotted as a function of pore size (Figure 7) and compared to some notable commercial membranes (represented by the red boxes, specific data in Table S3). At first glance, it might seem that order-of-magnitude flow rate enhancements do not simply translate in orders-of-magnitude higher permeability. In fact, the comparison, as presented has certain limitations that could be artificially depressing the real potential of CNT membranes: In the RO range, VA-CNT membranes where the CNTs have direct access to the water and are enclosed in a impermeable matrix (as those in [19, 39]) are assumed to repel salt ions purely by steric hindrance, unlike commercial polymeric RO membranes which are based on the solution-diffusion model (as well as Donnan exclusion) [14]. These membranes tend to have lower porosity than TFC RO membranes, depressing permeability. In fact, a ~3 order of magnitude higher permeability has been calculated, via MD, when the maximum packing density of CNTs in a VA-CNT membrane has been considered [19, 39]. This would push the permeability significantly above that of current commercial membranes if significant improvements in VA-CNT membrane manufacturing methods could be achieved [9]. It should also be noted that VA-CNT membranes tend to be much thicker than the active layer of commercial polymeric membranes, further penalizing them in the comparison. Unfortunately, most commercial membranes do not report the thickness of the active layer, so a comparison in terms of permeance could not be performed. As discussed in the introduction, in CNT-TFC membranes the tubes are embedded in the polymer active layer with random orientation, with only a fraction contributing to permeability. Hence the lower performance compared to the VA-CNT membranes.

In the NF range, CNT membranes, both vertically aligned and thin film composite ones, appear to significantly outperform commercial membranes. Many of the same considerations for nanotube membranes expressed in the RO range apply here. One potential difference, though somewhat controversial, is that for nanotube diameters above 2 nm there are both modelling [24, 31] and MD [40] results showing that the flow enhancement increases with increasing CNT length. This is attributed to the quasi-frictionless flow of water in the tubes and that, as the length increases, the entrance losses become smaller and smaller [41]. For example, the tubes in [4] are over 100 μm long, those in [6] about 200 μm and those in [5] are 4 mm long.

In the UF range, the boundaries of the box representing commercial membranes were particularly difficult to draw as commercial membranes typically report MWCO rather than pore sizes. This would lead to overstating the performance of commercial UF membranes, particularly close to the lower performance boundary. Therefore it is difficult to draw conclusions on the performance of the membranes prepared in this work as values straddle the commercial membranes boundary box. In this case a more appropriate comparison might be via MWCO tests [22]. Interestingly, the water permeability for one CNT-AAM, similar to those presented in this work, is about an order of magnitude higher [37] than what reported here. At least part of this difference can be attributed to differences in the surface structure and chemistry of the tubes that, in turn, affect flow, as per Eq. (5).

Results in Figure 7 point to the fact that, although orders of magnitude flow enhancement do not simply translate in orders of magnitude increases in permeability, there is significant potential for CNT membranes to outperform commercial ones. Thin film composite membranes containing randomly aligned tubes do not appear to have significantly higher permeability than commercial membranes in the RO range whereas vertically aligned ones clearly outperform them. The challenge, therefore, remains to invent a method to produce membranes with aligned tubes at a reasonable cost and with potential for large-scale production.

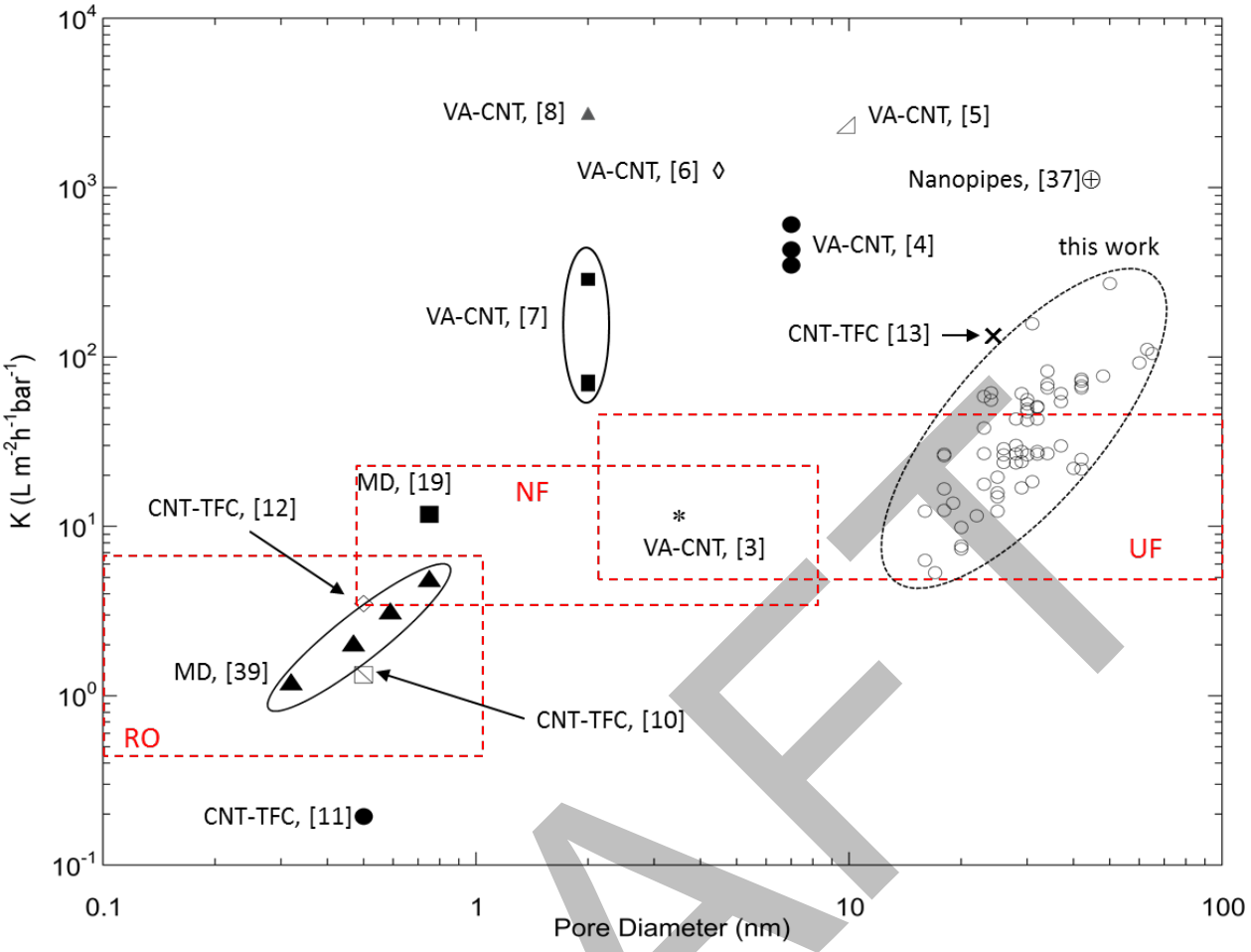

Figure 7. Permeability, K, as a function of nanotube / membrane pore diameter for this work (o) and for other nanotube membranes in the literature, including modeling and experimental results. The red boxes represent the performance boundaries for commercial polymeric membranes and should be used only for a qualitative comparison. Values for CNT-AMMs produced in this work can be found in Table S1; values for literature CNT membranes and commercial membranes can be found in Tables S2 and S3, respectively. Reference values correspond to those in the reference list.

3.4.1 Selectivity

While this paper is focussed on permeability, an analysis of the performance of nanotube membranes would not be complete without some discussion about selectivity. Unfortunately, there are much fewer results in the literature on this aspect to discuss. MD simulations of desalination through a carbon nanotube and a boron nitride nanotube showed complete salt rejection via steric hindrance and higher permeability compared to a corresponding PMMA nanotube, assumed to be representative of a polymeric RO membrane [42]. An interesting approach has been to use slightly larger nanotubes (resulting in higher permeability) with functional groups at the feed side to prevent salt ions from permeating while allowing the unobstructed flow of water molecules [19]. More recently thin film composite (TFC) membranes with randomly oriented CNTs incorporated in the active layer have shown a 4-fold flux improvement compared to the TFC baseline with no nanotubes while retaining similar salt rejection (~98.5) [10]. It is noted, though, that in this case the nanotubes are embedded in the polymer matrix and do not have direct access to the membrane surface. The enhanced transport occurs via the tubes inside the polymer matrix, with the precise mechanism still unclear.

4. Conclusions

The scope of this paper was to analyse water flow in carbon nanotube membranes in terms of permeability rather than flow enhancement, as the former is more useful than the latter when considering their potential use in any filtration application. A series of CNT membranes, prepared via non-catalytic CVD using anodic alumina templates (CNT-AAM) were characterized and tested to investigate the dependence of flow enhancement on the nanotubes' characteristic dimensions (diameter and length) and the strength of solid-liquid molecular interactions between the fluid and tube wall. By applying a recently developed model it was possible to derive an expression for the permeability as a function of solid-liquid molecular interactions. This expression is not limited to CNT membranes and can, in principle, be of general applicability. When the permeability of the CNT membranes produced in this work and of selected ones in the literature was compared to commercial membranes from RO to NF to UF, their performance, though appearing somewhat less promising than what the flow enhancement initially suggested, nonetheless shows that CNT membranes have significant potential to overcome current commercial membranes, at least in terms of pure water permeability.

Acknowledgement

The authors wish to acknowledge the UK EPSRC (grant number EP/G045798/1); DM also acknowledges the Royal Academy of Engineering for funding.

References

[1] M. Whitby, N. Quirke, Fluid Flow in Carbon Nanotubes and Nanopipes, Nat. Nano., 2 (2007) 87-94.
[2] D. Mattia, Y. Gogotsi, Review: static and dynamic behavior of liquids inside carbon nanotubes, Microfluid. Nanofluid., 5 (2008) 289-305.
[3] S. Kim, F. Fornasiero, H.G. Park, J.B. In, E. Meshot, G. Giraldo, M. Stadermann, M. Fireman, J. Shan, C.P. Grigoropoulos, O. Bakajin, Fabrication of flexible, aligned carbon nanotube/polymer composite membranes by in-situ polymerization, J. Membr. Sci., 460 (2014) 91-98.
[4] M. Majumder, N. Chopra, R. Andrews, B.J. Hinds, Nanoscale hydrodynamics: Enhanced Flow in Carbon Nanotubes, Nature, 438 (2005) 44.
[5] F. Du, L. Qu, Z. Xia, L. Feng, L. Dai, Membranes of Vertically Aligned Superlong Carbon Nanotubes, Langmuir, 27 (2011) 8437-8443.
[6] Y. Baek, C. Kim, D.K. Seo, T. Kim, J.S. Lee, Y.H. Kim, K.H. Ahn, S.S. Bae, S.C. Lee, J. Lim, K. Lee, J. Yoon, High performance and antifouling vertically aligned carbon nanotube membrane for water purification, J. Membr. Sci., 460 (2014) 171-177.
[7] J.K. Holt, H.G. Park, Y. Wang, M. Stadermann, A.B. Artyukhin, C.P. Grigoropoulos, A. Noy, O. Bakajin, Fast Mass Transport Through Sub-2-Nanometer Carbon Nanotubes, Science, 312 (2006) 1034-1037.
[8] M. Yu, H.H. Funke, J.L. Falconer, R.D. Noble, High Density, Vertically-Aligned Carbon Nanotube Membranes, Nano Lett., 9 (2008) 225-229.
[9] D. Mattia, K.P. Lee, F. Calabrò, Water permeation in carbon nanotube membranes, Current Opinion in Chemical Engineering, 4 (2014) 32-37.
[10] W.-F. Chan, H.-y. Chen, A. Surapathi, M.G. Taylor, X. Shao, E. Marand, J.K. Johnson, Zwitterion Functionalized Carbon Nanotube/Polyamide Nanocomposite Membranes for Water Desalination, ACS Nano, 7 (2013) 5308-5319.
[11] J.n. Shen, C.c. Yu, H.m. Ruan, C.j. Gao, B. Van der Bruggen, Preparation and characterization of thin-film nanocomposite membranes embedded with poly(methyl methacrylate) hydrophobic modified multiwalled carbon nanotubes by interfacial polymerization, J. Membr. Sci., 442 (2013) 18-26.
[12] H. Wu, B. Tang, P. Wu, Optimization, characterization and nanofiltration properties test of MWNTs/polyester thin film nanocomposite membrane, J. Membr. Sci., 428 (2013) 425-433.
[13] J.-H. Choi, J. Jegal, W.-N. Kim, Fabrication and characterization of multi-walled carbon nanotubes/polymer blend membranes, J. Membr. Sci., 284 (2006) 406-415.
[14] K.P. Lee, T.C. Arnot, D. Mattia, A review of reverse osmosis membrane materials for desalination--Development to date and future potential, J. Membr. Sci., 370 (2011) 1-22.

[15] M. Elimelech, W.A. Phillip, The Future of Seawater Desalination: Energy, Technology, and the Environment, Science, 333 (2011) 712-717.
[16] D. Mattia, H.H. Bau, Y. Gogotsi, Wetting of CVD Carbon Films by Polar and Non-Polar Liquids and Implications for Carbon Nanopipes, Langmuir, 22 (2006) 1789 -1794.
[17] D. Mattia, M.P. Rossi, B.M. Kim, G. Korneva, H.H. Bau, Y. Gogotsi, Effect of Graphitization on the Wettability and Electrical Conductivity of CVD Carbon Nanotubes and Films, J. Phys. Chem. B, 110 (2006) 9850 -9855.
[18] X. Sun, J. Wu, Z. Chen, X. Su, B.J. Hinds, Fouling Characteristics and Electrochemical Recovery of Carbon Nanotube Membranes, Adv Funct Mat, 23 (2013) 1500-1506.
[19] B. Corry, Water and ion transport through functionalised carbon nanotubes: implications for desalination technology, Energy & Environmental Science, 4 (2011) 751-759.
[20] K.P. Lee, H. Leese, D. Mattia, Water flow enhancement in hydrophilic nanochannels, Nanoscale, 4 (2012) 2621-2627.
[21] J.P. O'Sullivan, G.C. Wood, The Morphology and MEchanism of Formation of Porous Anodic Films on Aluminium, Proceed. R. Soc. Lond., 317 (1970) 511-543.
[22] K.P. Lee, D. Mattia, Monolithic nanoporous alumina membranes for ultrafiltration applications: Characterization, selectivity–permeability analysis and fouling studies, J. Membr. Sci., 435 (2013) 52-61.
[23] W.D. Harkins, Physical Chemistry of Surface Films, Reinhold, New York, 1952.
[24] D. Mattia, F. Calabrò, Explaining high flow rate of water in carbon nanotubes via solid–liquid molecular interactions, Microfluid. Nanofluid., 13 (2012) 125-130.
[25] H. Leese, D. Mattia, Electroosmotic flow in nanoporous membranes in the region of electric double layer overlap, Microfluid. Nanofluid., 16 (2014) 711-719.
[26] D. Mattia, G. Korneva, A. Sabur, G. Friedman, Y. Gogotsi, Multifunctional Carbon Nanotubes with Nanoparticles Embedded in their Walls, Nanotechnology, 18 (2007) 155305
[27] S. Sinha, M.P. Rossi, D. Mattia, Y. Gogotsi, H.H. Bau, Induction and measurement of minute flow rates through nanopipes, Phys. Fluids, 19 (2007) 013603-013608.
[28] E. Lauga, M.P. Brenner, H.A. Stone, Microfluidics: The No-Slip Boundary Condition, in: J. Foss, C. Tropea, A. Yarin (Eds.) Handbook of Experimental Fluid Dynamics, Springer, New York, 2005.
[29] C. Neto, D.R. Evans, E. Bonaccurso, H.-J. Butt, V.S.J. Craig, Boundary slip in Newtonian liquids: a review of experimental studies, Reports on Progress in Physics, 68 (2005) 2859-2897.
[30] F. Calabrò, K.P. Lee, D. Mattia, Modelling flow enhancement in nanochannels: Viscosity and slippage, Applied Mathematics Letters, 26 (2013) 991-994.
[31] K. Ritos, D. Mattia, F. Calabrò, J.M. Reese, Flow enhancement in nanotubes of different materials and lengths, J. Chem. Phys., 140 (2014).
[32] J.A. Thomas, A.J.H. McGaughey, Reassessing Fast Water Transport Through Carbon Nanotubes, Nano Lett., 8 (2008) 2788-2793.
[33] J.A. Thomas, A.J.H. McGaughey, O. Kuter-Arnebeck, Pressure-driven water flow through carbon nanotubes: Insights from molecular dynamics simulation, International Journal of Thermal Sciences, 49 (2010) 281-289.
[34] S. Joseph, N.R. Aluru, Why Are Carbon Nanotubes Fast Transporters of Water?, Nano Lett., 8 (2008) 452-458.
[35] J.H. Park, N.R. Aluru, Diffusion of water submonolayers on hydrophilic surfaces, Appl. Phys. Lett., 93 (2008) 253104.
[36] M.-J. Wei, J. Zhou, X. Lu, Y. Zhu, W. Liu, L. Lu, L. Zhang, Diffusion of water molecules confined in slits of rutile TiO2(1 1 0) and graphite(0 0 0 1), Fluid Phase Equilib., 302 (2011) 316-320.
[37] M. Whitby, L. Cagnon, M. Thanou, N. Quirke, Enhanced Fluid Flow through Nanoscale Carbon Pipes, Nano Lett., 8 (2008) 2632-2637.
[38] W.D. Nicholls, M.K. Borg, D.A. Lockerby, J.M. Reese, Water transport through carbon nanotubes with defects, Mol. Simul., 38 (2012) 781-785.
[39] B. Corry, Designing Carbon Nanotube Membranes for Efficient Water Desalination, The Journal of Physical Chemistry B, 112 (2007) 1427-1434.
[40] W. Nicholls, M. Borg, D. Lockerby, J. Reese, Water transport through (7,7) carbon nanotubes of different lengths using molecular dynamics, Microfluid. Nanofluid., 12 (2012) 257-264.
[41] T. Sisan, S. Lichter, The end of nanochannels, Microfluid. Nanofluid., (2011) 1-5.

[42] M.E. Suk, A.V. Raghunathan, N.R. Aluru, Fast reverse osmosis using boron nitride and carbon nanotubes, Appl. Phys. Lett., 92 (2008) 133120-133123.